

Interpreting Differences in Radiative Feedbacks from Aerosols Versus Greenhouse Gases

Pietro Salvi¹, Paulo Ceppi¹, Jonathan M. Gregory^{2,3}

¹Department of Physics & Grantham Institute, Imperial College London, London, UK

²National Centre for Atmospheric Science, University of Reading, Reading, UK

³Met Office Hadley Centre, Exeter, UK

Key Points:

- Effective climate sensitivity is larger (feedback more amplifying) for historical anthropogenic aerosol than greenhouse-gas forcing in CMIP6
- The key difference is that greenhouse-gas forcing is global, aerosol mainly extratropical (and aerosol hemispheric contrast unimportant)
- Extratropical forcing causes a shallower temperature response than tropical forcing, hence more positive cloud and lapse rate feedbacks

14 **Abstract**

15 Experiments with six CMIP6 models were used to assess the climate feedback parameter
 16 for net historical, historical greenhouse gas (GHG) and anthropogenic aerosol forcings.
 17 The net radiative feedback is found to be more amplifying (higher effective climate
 18 sensitivity) for aerosol than GHG forcing, and hence also more amplifying for net his-
 19 torical (GHG + aerosol) than GHG only. We demonstrate that this difference is con-
 20 sistent with their different latitudinal distributions. Historical aerosol forcing is most pro-
 21 nounced in northern extratropics, where the boundary layer is decoupled from the free
 22 troposphere, so the consequent temperature change is confined to low altitude and causes
 23 low-level cloud changes. This is caused by change in stability which also affects upper-
 24 tropospheric clearsky emission, both affecting shortwave and longwave radiative feed-
 25 backs. This response is a feature of extratropical forcing generally, regardless of its sign
 26 or hemisphere.

27 **Plain Language Summary**

28 Understanding how the Earth's surface temperatures change in accordance with
 29 the anomalous energy flow into the system due to changes in greenhouse gases (GHGs)
 30 or anthropogenic aerosols is vital for predicting future temperature change. New data
 31 has made it possible to better calculate how efficiently the planet responds to temper-
 32 ature change (so as to return to energy equilibrium) for historical aerosols and GHGs.
 33 We find that the Earth requires greater surface temperature changes under aerosol cli-
 34 mate forcing than it does for GHGs in order to balance out incoming and outgoing en-
 35 ergy into the Earth system. By comparing with experiments that prescribe energy changes
 36 only outside the tropics, we find that the lower efficiency of aerosols is related to their
 37 being mainly located away from the equator, unlike GHGs which are generally well mixed
 38 throughout the globe. This forcing away from the equator is tied to the vertical distri-
 39 bution of temperature changes, which in turn affects how efficiently surface temperature
 40 change leads to balancing the incoming and outgoing energy into the Earth system, lead-
 41 ing to different temperature changes for the same global average forcings.

42 **1 Introduction**

43 Global warming due to future emissions of greenhouse gases and other climate forc-
 44 ing agents has been understood in recent years in terms of the energy imbalance that
 45 these forcings cause in the Earth system, to which this system responds through chang-
 46 ing surface temperatures. The usual interpretive model is $N = F - \alpha T$, where α is the
 47 climate feedback parameter, N top-of-atmosphere energy imbalance, T global mean sur-
 48 face temperature change and F effective radiative forcing (Ramaswamy et al., 2001). (Note:
 49 we have chosen the sign convention where a positive α implies an increased positive-upwards
 50 radiative response for increasing surface temperatures.) Although this is helpful and in-
 51 tuitive as a simple model, there are several complications when using it (Andrews et al.,
 52 2015; Knutti & Rugenstein, 2015; Sherwood et al., 2015).

53 While there are generally confirmed differences in the feedback parameter across
 54 models (Andrews et al., 2012; Becker & Wing, 2020; Zelinka et al., 2020), there is not
 55 a consensus on whether α depends on the different forcing agents that are relevant to
 56 past and future temperature changes. Comparing aerosols and GHGs, the two dominant
 57 historical forcing agents (Smith et al., 2020), several studies have found differences in
 58 feedbacks (Marvel et al., 2016; Shindell, 2014). Gregory et al. (2020) presented evidence
 59 for a difference in α between anthropogenic forcing (GHGs and aerosols) and natural forc-
 60 ing by volcanic aerosol. However, Richardson et al. (2019) did not find significant dif-
 61 ferences among forcing agents, considering several models in the Precipitation Driver Model
 62 Intercomparison Project (PDRMIP) experiments. The focus of this study is the depen-
 63 dence of α on the nature of the forcing agent.

In the recently released data of the Coupled Model Intercomparison Project phase 6 (CMIP6), historical single-forcing experiments across several models have become available for analysis. These new experiments allow us to obtain the effective forcings for different agents, allowing us to accurately calculate the corresponding radiative feedbacks over the historical period. Since previous work has found a dependence on forcing patterns (Andrews et al., 2015; Ceppi & Gregory, 2019; Zhou et al., 2017), which affect the radiation budget via changes in stability and clouds (Andrews et al., 2018), this work considers stability responses to historical greenhouse gases versus historical aerosols and how these correlate with the radiative responses. To do this, we analyse the upward TOA radiative response R , the stability response S as measured by the estimated inversion strength (EIS; Wood & Bretherton, 2006), and the cloud-radiative effect (CRE) measured as the difference in allsky versus clearsky downward fluxes.

2 Methods

Data for several historical forcing experiments was obtained from the ESGF CEDA archive (esgf-index1.ceda.ac.uk) for six models: CanESM5, GISS-E2-1-G, HadGEM3-GC31-LL, IPSL-CM6A-LR, MIROC6, and NorESM2-LM. These experiments include a control (pi-Control) with constant pre-industrial forcing agents, as well as experiments both with coupled atmosphere-ocean models (AOGCMs) and with atmosphere models (AGCMs) given prescribed sea surface conditions, for historical GHGs, aerosols, and all historical forcings together. The different variants which had the required data are detailed in Table S1. Where possible, we chose variants with the same initialisation (i1 variant label), physics and forcing definition as in piControl. We included all realisations that contained all of the required variables, and our results from each experiment of each model are ensemble averages. We calculate multi-model mean (MMM) values from the individual model ensemble averages, with equal weighting for each model.

Prior to analysis, all fields were regridded to a common T42 grid (corresponding to a grid resolution of approximately 2.8° in longitude and latitude), using conservative remapping for radiative fluxes, and bilinear interpolation for other fields. Monthly fields were aggregated into annual averages.

In order to separate out the surface warming (or cooling) driven feedbacks from the forcing and associated rapid adjustments (Hansen et al., 1997; Sherwood et al., 2015), we use the results from the AGCM experiments with fixed sea surface temperatures through the following equation:

$$X_{\text{agent}} = X_{\text{AOGCM}} - X_{\text{AGCM}}, \quad (1)$$

where X represents the variable of interest. Radiative feedbacks and other responses per unit global warming were calculated through linear least-squares regression of the desired variable against global-average surface air temperature.

The confidence intervals for results derived from regressions combine two aspects of uncertainty. The first is the variability among different ensemble members, which we have calculated for each model as the variance across members of the historical experiment. This experiment was chosen since it generally had the most ensemble members, with the assumption that the magnitude of unforced variability is representative of other forcing scenarios. The second is the estimated error in the regression slope of the ensemble-averaged data. The combined error is calculated as the square root of the sum of variances from these two aspects of uncertainty, so they correspond to $\pm 1\sigma$ of the probability distribution.

Two idealised extratropical forcing experiments were run to investigate the impact of forcing localised away from the regions of deep convection on radiative feedbacks and tropospheric stability. These experiments are denoted as nh_extrop and sh_extrop for northern (30°N – 90°N) and southern (30°S – 90°S) hemisphere forcing respectively. A uniform

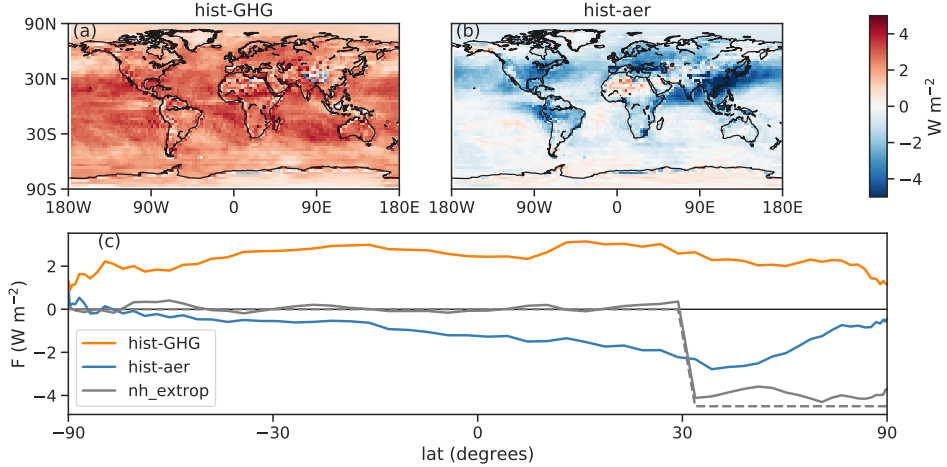


Figure 1. Top-of-atmosphere radiative forcing patterns over years 1995–2014 for hist-GHG (a) and hist-aer (b). The zonal-mean profiles of forcing are shown in (c), where values for hist-GHG (orange) and hist-aer (blue) are the average effective forcings of the relevant AGCM experiments (piClim-histghg and piClim-histaer, respectively) minus control. For nh_extrop (grey) the dashed line shows the prescribed instantaneous forcing whilst the solid line shows the effective forcing calculated from the HadAM3 (atmosphere-only) simulation. Note that the *x*-axis is scaled by geographical area.

“ghost” radiative forcing of -4.5 W m^{-2} was imposed as an extra term in the surface energy budget in the relevant regions for each experiment. The imposed instantaneous radiative flux values were chosen so that the global average forcing would be comparable to that of hist-aer over years 1995–2014 (around 1.13 W m^{-2}). Though the nh_extrop forcing is zonally uniform unlike the forcing for hist-GHG and hist-aer (Fig. 1a-b), the nh_extrop setup was chosen to capture the skew of the northern extratropical forcing that is seen in hist-aer relative to the more homogeneous hist-GHG (Fig. 1c). The idealised experiments were performed with the Hadley Centre Atmospheric Model version 3 (Pope et al., 2000) in both atmosphere-only (HadAM3) and slab ocean (HadSM3) configurations. The horizontal resolution is $2.5^\circ \times 3.75^\circ$; there are 19 levels in the atmosphere and the slab ocean has a thickness of 50 m. This model is one of the two used by Cessi and Gregory (2019), and these experiments are the same as their $-\text{UNIF}_{\text{ET}}$ experiment for a single hemisphere at a time, except with a different forcing magnitude.

We also make use of tropical-only forcing experiments in HadSM3 and HadAM3 denoted as “tropical” in later figures. This is the same as the $+\text{UNIF}_{\text{T}}$ experiment in Cessi and Gregory (2019), which involves a uniform forcing of 7 W m^{-2} over the tropics (30°S - 30°N).

3 Investigating radiative feedback differences in terms of stability differences

The radiative feedbacks for historical aerosol and all historical forcings, relative to those from GHGs, are shown in Fig. 2a, for each model analysed and for the MMM. Coloured bars show the allsky net feedback parameter α , whilst markers show the CRE feedback parameter α_{CRE} (minuses) and clearsky feedback parameter α_{CS} (pluses). In all cases, positive numbers mean less amplifying feedbacks, i.e. a relatively larger upward radia-

133 tive flux perturbation for positive T . The findings here show more amplifying feedbacks
 134 for hist-aer than hist-GHG in the MMM. On a model-by-model basis, hist-aer shows ei-
 135 ther significantly more amplifying or very similar feedbacks to hist-GHG. Neither α_{CS}
 136 (correlation of 0.82 with allsky α , Fig. S1b) nor α_{CRE} (correlation of 0.88 with allsky α ,
 137 Fig. S1d) entirely explains the differences of allsky α for aerosol (or the all historical)
 138 compared to GHG forcing, despite correlations here being highly significant ($p < 0.001$).

139 We propose that differences in radiative feedback across forcing agents may be ex-
 140 plained in terms of different tropospheric stability responses and their impact on cloud
 141 and lapse-rate feedbacks. Fig. 2b shows that hist-aer causes lower stability responses than
 142 hist-GHG across all models. A greater increase in stability (as in GHG compared with
 143 aerosol) means more warming in the upper troposphere than at the surface, and hence
 144 a negative (less amplifying) lapse-rate feedback (Andrews & Webb, 2018; Ceppi & Gre-
 145 gory, 2019). Furthermore, tropospheric stability is a key variable for cloud formation,
 146 with higher stability encouraging the formation of low boundary-layer clouds over ma-
 147 rine regions (Zhou et al., 2016; Ceppi et al., 2017; Andrews & Webb, 2018; Ceppi & Gre-
 148 gory, 2019). Low clouds have little impact on outgoing longwave radiation due to their
 149 temperatures being similar to those at the surface. Since they reflect incoming solar ra-
 150 diation, however, low clouds have an overall positive upwards (cooling) effect on radi-
 151 ation (Hartmann, 1994). Positive forcings that increase stability will thus tend to pro-
 152 mote low-level cloudiness and give a positive upwards radiative feedback that opposes
 153 the forcing. The feedbacks from increased low cloud, combined with lapse-rate feedbacks,
 154 are why we expect a positive correlation between net α and the stability response
 155 S per unit global warming, which we refer to as dS/dT .

156 Figure 2c–g supports this inference. Considering all models and experiments to-
 157 gether, there is a strong positive correlation between net α and dS/dT (0.72 for the AOGCM
 158 experiments, Fig. 2c). Much of the spread in α among this set of models is related to
 159 stability, despite our expectation that inter-model differences in climate feedback are dom-
 160 inated by cloud responses to mean SST warming (Ringer et al., 2014). This is still the
 161 case when feedbacks are broken down into α_{CS} (Fig. 2e) and, though to a lesser extent,
 162 α_{CRE} (Fig. 2g). We interpret the correlation in Fig. 2e as being primarily driven by the
 163 linkage between stability and lapse-rate feedbacks (Andrews & Webb, 2018; Ceppi & Gre-
 164 gory, 2019).

165 By instead considering differences of α in each model of hist-aer and historical from
 166 hist-GHG, we remove the model spread, revealing the positive correlation (Fig. 2d) be-
 167 tween α and stability change in response to different forcing agents. Although the cor-
 168 relation across models is not very strong (0.65) it is highly significant ($p = 0.001$), and the
 169 relationship is significant in the MMM according to estimated error bars. The lack of
 170 correlation in Fig. 2h, both across models and in the MMM, despite such correlation in
 171 Fig. 2f, suggests that the impacts of stability on lapse-rate feedbacks are more robust
 172 than the impacts on α_{CRE} for explaining differences in α between historical aerosols and
 173 GHGs. This may be because the relationship between S and CRE is not consistently sim-
 174 ultated among climate models. Alternatively, it is possible that contrary to the findings
 175 of Ceppi and Gregory (2019), global stability changes are not strongly physically linked
 176 to CRE in some of the models, and that regional changes in S would be a better explana-
 177 tory factor.

178 The historical all-forcing case is dominated by responses to GHGs and aerosols (Smith
 179 et al., 2020). Therefore, differences between historical and hist-GHG experiments are due
 180 to differences between hist-aer and hist-GHG. Both the feedback parameter (Fig. 2a) and
 181 the stability response (Fig. 2b) are greater for historical than for hist-GHG in the MMM.
 182 This results from combining hist-GHG and hist-aer responses, given that aerosols and
 183 GHGs forcing are of opposite sign (Appendix B in the online supporting information of
 184 Gregory and Andrews, 2016). A visual explanation of it can be found in Fig. S2.

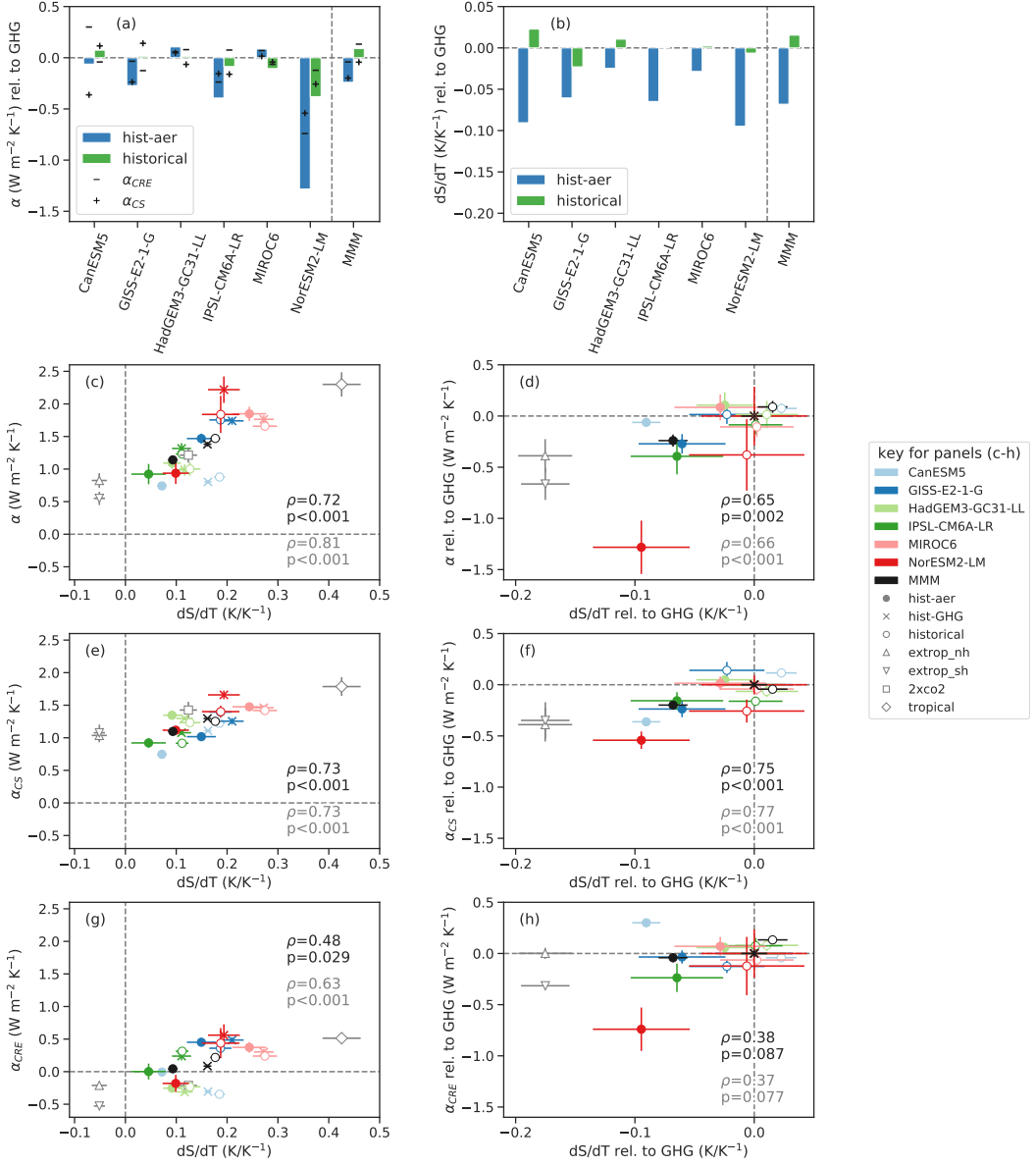


Figure 2. (a) allsky radiative feedback parameter (α , bars) alongside CRE (α_{CRE} , minuses) and clearsky radiative feedback parameters (α_{CS} , pluses) for each model and the multi-model mean, as the difference from hist-GHG values. (b) Difference of dS/dT from hist-GHG values. (c,e,g) Net (c) clearsky, (e) CRE, and (g) allsky radiative feedback parameters against net dS/dT . (d,f,h) as row above, except with values relative to hist-GHG. Confidence intervals in (c-h) denote \pm one standard deviation based off combined regression and ensemble member uncertainties. The Pearson correlation ρ is shown in (c-h), across models and both excluding (black) and including (grey) the data points from the HadSM3 experiments. The tropical-only forcing experiment is included in (c,e,g), as part of the inter-model trend, but excluded (both in plotting and ρ) in (d,f,h) for clarity and to focus on the HadSM3 experiments that are more similar to hist-aer and hist-GHG. Also shown are p -values for the statistical significance of the correlations.

The results here are in agreement with findings from previous studies of a greater transient climate response (indicative of a less positive α) from aerosols (Marvel et al., 2016) and extratropical forcing (Rose et al., 2014; Rose & Rayborn, 2016; Shindell, 2014) compared to forcing from well-mixed GHGs. By contrast, Richardson et al. (2019) found no significant differences in feedback between two kinds of aerosol (SO_4 and BC) and GHGs, regardless of whether they calculated ERF as in the present paper, or additionally correcting for the impact of land surface temperature adjustments (Andrews et al., 2021). There are several possible explanations for our disagreement, including the following. (1) Despite its statistical significance, the difference we find between feedbacks to aerosol and GHG forcing may be specific to our selection of models, which is smaller than theirs (6, versus 11 in PDRMIP models). (2) Historical aerosol and the 5xSO_4 forcing in PDRMIP might have important differences in feedback, because the contributions of other aerosols than SO_4 are not negligible, although SO_4 forcing is predominant (Myhre et al., 2014). (3) The feedback for a step-like five-fold increase in control SO_4 concentration (as in PDRMIP) may differ from that for the smaller historical SO_4 increases.

200 4 Explaining stability differences in hist-aer in terms of extratropical 201 forcing

202 Next, we interpret the distinct radiative and stability responses to aerosols and GHGs
203 in terms of the latitudinal distribution of forcing. Ceppi and Gregory (2019) demonstrated
204 that positive tropical forcing tends to increase global stability per unit global surface warming,
205 while positive extratropical forcing has the opposite impact (and vice versa for neg-
206 ative forcing). To understand why, we recall that the tropics are generally well-coupled
207 to the free troposphere, with the lapse rate closely following a moist adiabat due to moist
208 convection (Flannaghan et al., 2014; Sobel, 2002). Consequently, tropical warming has
209 a relatively large impact on free-tropospheric temperature. Mixing by atmospheric mo-
210 tions propagates the warming signal to the extratropical free troposphere, stabilising the
211 atmosphere there (Fig. 3d). Conversely, positive forcing in the extratropics is expected
212 to decrease stability, since surface temperature in the extratropics is more weakly cou-
213 pled to the free troposphere. The effects of extratropical surface forcing tend to be more
214 confined near to the surface, and since this forcing acts on a region that is (on average)
215 climatologically stable, the stability response is similar to that found for warming in other
216 stable regions such as in the tropical South-East Pacific (Andrews & Webb, 2018). This
217 effect can be seen by comparing air temperature changes in the hist-aer and hist-GHG
218 cases (Fig. 3e). Note that aerosol forcing is *negative* and causes a surface *cooling*, but
219 the patterns in Fig. 3 are normalised by regression against global mean surface temper-
220 ature change, and the sign of dS/dT is unaffected.

221 This reasoning could explain why the hist-aer case gives a less positive stability re-
222 sponse per unit surface warming than the hist-GHG case. The skew of forcing towards
223 the extratropics in the hist-aer case (blue line in Fig. 1c) means that a relatively larger
224 fraction of the surface temperature response is in vertically decoupled regions, leading
225 to the smaller dS/dT than in hist-GHG. In support of this hypothesis, we note that the
226 pattern of tropospheric temperature change in the HadSM3 nh_extrop experiment com-
227 pared to the 2xco2 experiment (Fig. 3g) is similar to the difference between hist-aer and
228 hist-GHG (Fig. 3e). The pattern from tropical-only forcing (Fig. 3d) shows the prop-
229 agation of warming to both the tropical and extratropical free tropospheres in accordance
230 with an increase to stability as seen in Fig. 2c–g. Fig. 2e shows that dS/dT is negative
231 for both nh_extrop and sh_extrop, whereas it is positive in nearly every historical forc-
232 ing experiment. This difference is probably related to the absence of tropical forcing in
233 the idealised cases. That the negative dS/dT occurs for forcing in both hemispheres sug-
234 gests that the essential characteristic is that the forcing is extratropical, rather than hemi-
235 sppheric. The historical all-forcing case shows the opposite pattern to hist-aer when com-

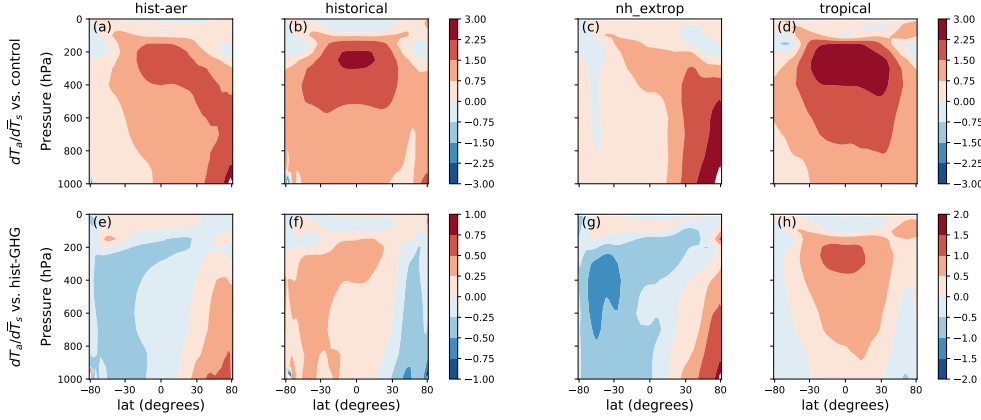


Figure 3. MMM zonal-mean profiles of local air temperature regressed onto global surface air temperature. Values shown are absolute (a–b), and relative to hist-GHG (e–f). Also shown are the results from the HadSM3 NH extratropical forcing (c) and tropical-only forcing (d), and these relative to the HadSM3 2xco₂ experiment (g–h). Note that the *x*-axis is scaled by geographical area.

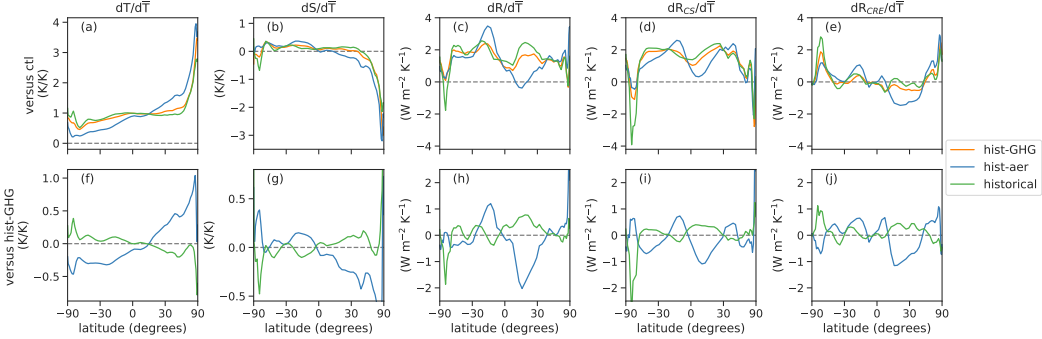


Figure 4. MMM zonal-mean values regressed onto global surface air temperature for the historical cases (*top row*) and differenced relative to hist-GHG (*bottom row*) in terms of (a,e) temperature, (b,f) estimated inversion strength, (c,g) net upwards radiative response, (d,h) upwards radiative response in clearsky and (e,i,j) upwards radiative response from CRE. Note that the *x*-axis is scaled by geographical area.

pared to hist-GHG (Fig. 3e–f), indicating that aerosol has a similar effect on stability whether applied independently or jointly with GHGs.

To corroborate this reasoning, we consider the MMM zonal means of feedbacks and climate responses in Fig. 4. There is less meridional contrast in response to hist-GHG than hist-aer (top row). Subtracting the responses from hist-GHG (bottom row), we see a positive NH temperature response per unit global warming in hist-aer relative to hist-GHG, and the opposite in the SH. This anti-correlates with the stability response per unit surface warming, which in turn correlates (in low latitudes) with the radiative response. The radiative response is then finally well explained, in terms of pattern, by the combination of clearsky and CRE feedbacks.

Just as the global average feedbacks for the historical case are more positive than those for hist-GHG, the zonal-mean curves for hist-GHG generally lie between those for

248 the all historical and hist-aer cases (top row of Fig. 4), again consistent with the expected
 249 effect of aerosol. Likewise, the difference between historical and hist-GHG responses (bot-
 250 tom row of Fig. 4) can be interpreted as representing the effect of aerosol, but with the
 251 sign reversed (see Appendix A in the Supporting Information).

252 5 Summary and Conclusions

253 Our analysis of AOGCM historical experiments from CMIP6 (including new ex-
 254 periments which allow forcing to be diagnosed) reveals that climate feedback is more strongly
 255 amplifying (greater climate sensitivity) in response to anthropogenic aerosol forcing than
 256 greenhouse-gas (GHG) forcing. This difference is shown and is statistically significant
 257 in the MMM, though only six AOGCMs have so far provided the required historical ex-
 258 periments and variables for this analysis, so it would be useful to repeat it with more.
 259 Our finding is consistent with those from past studies that also found greater climate
 260 sensitivity to aerosol than GHGs (Marvel et al., 2016; Shindell, 2014), but appears in-
 261 consistent with the recent study of Richardson et al. (2019). Further work is needed to
 262 explain the disagreement, which may relate to differences in the details of the prescribed
 263 aerosol forcing (e.g. SO₄ only or a mixture of type of aerosol, historical concentration
 264 changes or the fivefold increase prescribed by Richardson et al.).

265 Furthermore, we find that the difference in (positive-stable) net top-of-atmosphere
 266 radiative feedback parameter for aerosol and GHG forcing is positively correlated across
 267 AOGCMs with a difference in the response of tropospheric stability to the two kinds of
 268 forcing. We propose that the difference arises from the different latitudinal distributions
 269 of the forcing. An idealised slab model experiment with uniform surface forcing confined
 270 to the Northern extratropics qualitatively reproduces the near-surface extratropical tem-
 271 perature change that differentiates the historical aerosol experiment from the historical
 272 GHG experiment. The shallower extratropical temperature change in the former is ex-
 273 plained by the lower proportion of forcing in the tropics, where the surface is relatively
 274 strongly coupled to the free troposphere by deep convection (Flannaghan et al., 2014;
 275 Sobel, 2002), compared to the higher proportion of forcing in the extratropics, where the
 276 coupling is weaker and the effect of forcing more confined to the surface.

277 Thus a positive extratropical forcing causes a near-surface warming, which reduces
 278 tropospheric stability, whereas a positive tropical forcing has less effect on stability. A
 279 reduction in stability tends to reduce low-level cloudiness, which gives an anomalously
 280 positive shortwave feedback on warming, whilst it also induces an anomalously positive
 281 longwave lapse-rate feedback. In this way, the latitude of forcing is linked to the radi-
 282 ative feedback it produces. Historical aerosol forcing is negative, so the signs of temper-
 283 ature and stability change are reversed, but the feedback parameter, sensitivity of sta-
 284 bility (change per unit warming), and hence the correlation with the feedback param-
 285 eter have the same sign for either sign of forcing: extratropical forcing tends to give higher
 286 climate sensitivity. This link accords with previous works that have highlighted the im-
 287 pact of forcing patterns on radiative feedbacks (Ceppi & Gregory, 2019; Rose et al., 2014;
 288 Rose & Rayborn, 2016).

289 Historical climate change is dominated by GHG forcing. Hence the net feedback
 290 simulated in the historical experiments with all forcings is nearer to that for GHG than
 291 for anthropogenic aerosol. The effective climate sensitivity for historical forcing is slightly
 292 *smaller* than for historical GHG forcing (the magnitude of α is larger), because of in-
 293 cluded historical aerosol forcing, for which climate sensitivity is *larger*, but the sign is
 294 opposite. We find also that some of the spread across AOGCMs in the climate sensitiv-
 295 ity to GHG forcing is also correlated with the response of tropospheric stability to forc-
 296 ing; this aspect is intriguing and requires further investigation.

297 **Acknowledgments**

298 PS was supported by the Department of Physics and the Grantham Institute of Impe-
 299 rial College London. PC was supported by an Imperial College Research Fellowship and
 300 NERC grants NE/T006250/1 and NE/T007788/1. JMG was supported by the European
 301 Research Council under the European Union's Horizon 2020 research and innovation pro-
 302 gramme (grant agreement No 786427, project "Couplet"). This work used JASMIN, the
 303 UK collaborative data analysis facility and the ARCHER UK National Supercomput-
 304 ing Service. The data that support the findings of this study are available online. The
 305 data from CMIP6 experiments can be found on the ESGF CEDA node available at `esgf-`
 306 `-index1.ceda.ac.uk`. The data from the HadSM3 and HadAM3 experiments can be
 307 found at
 308 <https://doi.org/10.6084/m9.figshare.17197748> and
 309 <https://doi.org/10.6084/m9.figshare.17182907>.

310 **References**

- 311 Andrews, T., Gregory, J. M., Paynter, D., Silvers, L. G., Zhou, C., Mauritsen,
 312 T., ... Titchner, H. (2018). Accounting for Changing Temperature Pat-
 313 terns Increases Historical Estimates of Climate Sensitivity. *Geophysical Re-
 314 search Letters*, 45(16), 8490–8499. Retrieved 2019-07-15, from <https://agupubs.onlinelibrary.wiley.com/doi/abs/10.1029/2018GL078887> doi:
 315 10.1029/2018GL078887
- 316 Andrews, T., Gregory, J. M., & Webb, M. J. (2015, February). The Dependence of
 317 Radiative Forcing and Feedback on Evolving Patterns of Surface Temperature
 318 Change in Climate Models. *Journal of Climate*, 28(4), 1630–1648. Retrieved
 319 2021-12-09, from <https://journals.ametsoc.org/view/journals/clim/28/4/jcli-d-14-00545.1.xml> (Publisher: American Meteorological Society
 320 Section: Journal of Climate) doi: 10.1175/JCLI-D-14-00545.1
- 321 Andrews, T., Gregory, J. M., Webb, M. J., & Taylor, K. E. (2012). Forcing,
 322 feedbacks and climate sensitivity in CMIP5 coupled atmosphere-ocean cli-
 323 mate models. *Geophysical Research Letters*, 39(9). Retrieved 2019-07-23,
 324 from <https://agupubs.onlinelibrary.wiley.com/doi/abs/10.1029/2012GL051607> doi: 10.1029/2012GL051607
- 325 Andrews, T., Smith, C. J., Myhre, G., Forster, P. M., Chadwick, R., & Ack-
 326 erley, D. (2021). Effective Radiative Forcing in a GCM With Fixed
 327 Surface Temperatures. *Journal of Geophysical Research: Atmo-
 328 spheres*, 126(4), e2020JD033880. Retrieved 2021-10-29, from <https://onlinelibrary.wiley.com/doi/abs/10.1029/2020JD033880> (.eprint:
 329 <https://onlinelibrary.wiley.com/doi/pdf/10.1029/2020JD033880>) doi:
 330 10.1029/2020JD033880
- 331 Andrews, T., & Webb, M. J. (2018, January). The Dependence of Global Cloud and
 332 Lapse Rate Feedbacks on the Spatial Structure of Tropical Pacific Warming.
 333 *Journal of Climate*, 31(2), 641–654. Retrieved 2021-10-12, from <https://journals.ametsoc.org/view/journals/clim/31/2/jcli-d-17-0087.1.xml>
 334 (Publisher: American Meteorological Society Section: Journal of Climate) doi:
 10.1175/JCLI-D-17-0087.1
- 335 Becker, T., & Wing, A. A. (2020). Understanding the Extreme Spread in Cli-
 336 mate Sensitivity within the Radiative-Convective Equilibrium Model In-
 337 tercomparison Project. *Journal of Advances in Modeling Earth Systems*,
 338 12(10), e2020MS002165. Retrieved 2020-11-11, from <https://agupubs.onlinelibrary.wiley.com/doi/abs/10.1029/2020MS002165> (.eprint:
 339 <https://agupubs.onlinelibrary.wiley.com/doi/pdf/10.1029/2020MS002165>) doi:
 340 <https://doi.org/10.1029/2020MS002165>
- 341 Ceppi, P., Brent, F., Zelinka, M. D., & Hartmann, D. L. (2017). Cloud feedback
 342 mechanisms and their representation in global climate models. *Wiley Inter-*

- 350 *disciplinary Reviews: Climate Change*, 8(4), e465. Retrieved 2019-07-15,
 351 from <https://onlinelibrary.wiley.com/doi/abs/10.1002/wcc.465> doi:
 352 10.1002/wcc.465
- 353 Ceppi, P., & Gregory, J. M. (2019, October). A refined model for the Earth's global
 354 energy balance. *Climate Dynamics*, 53(7), 4781–4797. Retrieved 2020-12-03,
 355 from <https://doi.org/10.1007/s00382-019-04825-x> doi: 10.1007/s00382
 356 -019-04825-x
- 357 Flannaghan, T. J., Fueglistaler, S., Held, I. M., Po-Chedley, S., Wyman,
 358 B., & Zhao, M. (2014). Tropical temperature trends in Atmo-
 359 spheric General Circulation Model simulations and the impact of un-
 360 certainties in observed SSTs. *Journal of Geophysical Research: Atmo-*
 361 *spheres*, 119(23), 13,327–13,337. Retrieved 2021-10-12, from <https://onlinelibrary.wiley.com/doi/abs/10.1002/2014JD022365> (_eprint:
 362 <https://onlinelibrary.wiley.com/doi/pdf/10.1002/2014JD022365>) doi:
 363 10.1002/2014JD022365
- 364 Hansen, J., Sato, M., & Ruedy, R. (1997). Radiative forcing and climate response.
 365 *Journal of Geophysical Research: Atmospheres*, 102(D6), 6831–6864. Retrieved
 366 2019-08-09, from <https://agupubs.onlinelibrary.wiley.com/doi/abs/10.1029/96JD03436> doi: 10.1029/96JD03436
- 367 Hartmann, D. L. (1994). *Global physical climatology*. San Diego ; London: Academic
 368 Press.
- 369 Knutti, R., & Rugenstein, M. A. A. (2015, November). Feedbacks, climate sen-
 370 sitivity and the limits of linear models. *Philosophical Transactions of the Royal Society A: Mathematical, Physical and Engineering Sciences*, 373(2054), 20150146. Retrieved 2019-07-15, from <https://royalsocietypublishing.org/doi/full/10.1098/rsta.2015.0146> doi: 10.1098/rsta.2015.0146
- 371 Marvel, K., Schmidt, G. A., Miller, R. L., & Nazarenko, L. S. (2016, April).
 372 Implications for climate sensitivity from the response to individual forc-
 373 ings. *Nature Climate Change*, 6(4), 386–389. Retrieved 2021-10-08, from
 374 <https://www.nature.com/articles/nclimate2888> (Bandiera_abtest: a
 375 Cg_type: Nature Research Journals Number: 4 Primary_atype: Research
 376 Publisher: Nature Publishing Group Subject_term: Climate and Earth sys-
 377 tem modelling;Projection and prediction Subject_term_id: climate-and-earth-
 378 system-modelling;projection-and-prediction) doi: 10.1038/nclimate2888
- 379 Myhre, G., Shindell, D., Bréon, F.-M., Collins, W., Fuglestvedt, J., Huang,
 380 J., ... Zhang, H. (2014). *Anthropogenic and Natural Radiative Forc-*
 381 *ing. In: Climate Change 2013: The Physical Science Basis. Contribution*
 382 *of Working Group I to the Fifth Assessment Report of the Intergovern-*
 383 *mental Panel on Climate Change* (Tech. Rep. No. AR5). Retrieved from
 384 <https://www.ipcc.ch/report/ar5/wg1/> (Publisher: Cambridge University
 385 Press)
- 386 Pope, V. D., Gallani, M. L., Rowntree, P. R., & Stratton, R. A. (2000, Febru-
 387 ary). The impact of new physical parametrizations in the Hadley Cen-
 388 tre climate model: HadAM3. *Climate Dynamics*, 16(2), 123–146. Re-
 389 trieved 2021-10-22, from <https://doi.org/10.1007/s003820050009> doi:
 390 10.1007/s003820050009
- 391 Ramaswamy, V., Boucher, O., Haigh, J., Hauglustaine, D., Haywood, J., Myhre, G.,
 392 ... Srinivasan, J. (2001). *Radiative Forcing of Climate Change* (Tech. Rep.).
 393 IPCC, Geneva, Switzerland. Retrieved from <https://www.ipcc.ch/site/assets/uploads/2018/03/TAR-06.pdf>
- 394 Richardson, T. B., Forster, P. M., Smith, C. J., Maycock, A. C., Wood, T., An-
 395 drews, T., ... Watson-Parris, D. (2019). Efficacy of Climate Forcings in
 396 PDRMIP Models. *Journal of Geophysical Research: Atmospheres*, 124(23),
 397 12824–12844. Retrieved 2020-01-17, from <https://agupubs.onlinelibrary.wiley.com/doi/abs/10.1029/2019JD030581> doi: 10.1029/2019JD030581

- 405 Ringer, M. A., Andrews, T., & Webb, M. J. (2014). Global-mean radiative
 406 feedbacks and forcing in atmosphere-only and coupled atmosphere-
 407 ocean climate change experiments. *Geophysical Research Letters*, 41(11), 4035–4042.
 408 Retrieved 2021-10-22, from <https://onlinelibrary.wiley.com/doi/abs/10.1002/2014GL060347> (.eprint:
 409 <https://onlinelibrary.wiley.com/doi/pdf/10.1002/2014GL060347>) doi:
 410 10.1002/2014GL060347
- 412 Rose, B. E. J., Armour, K. C., Battisti, D. S., Feldl, N., & Koll, D. D. B.
 413 (2014). The dependence of transient climate sensitivity and radiative
 414 feedbacks on the spatial pattern of ocean heat uptake. *Geophysical Re-*
 415 *search Letters*, 41(3), 1071–1078. Retrieved 2021-11-01, from <https://onlinelibrary.wiley.com/doi/abs/10.1002/2013GL058955> (.eprint:
 416 <https://onlinelibrary.wiley.com/doi/pdf/10.1002/2013GL058955>) doi:
 417 10.1002/2013GL058955
- 419 Rose, B. E. J., & Rayborn, L. (2016, December). The Effects of Ocean Heat Uptake
 420 on Transient Climate Sensitivity. *Current Climate Change Reports*, 2(4), 190–
 421 201. Retrieved 2021-11-01, from <http://link.springer.com/10.1007/s40641-016-0048-4> doi: 10.1007/s40641-016-0048-4
- 423 Sherwood, S. C., Bony, S., Boucher, O., Bretherton, C., Forster, P. M., Gregory,
 424 J. M., & Stevens, B. (2015, February). Adjustments in the Forcing-Feedback
 425 Framework for Understanding Climate Change. *Bulletin of the American
 426 Meteorological Society*, 96(2), 217–228. Retrieved 2020-12-10, from <https://journals.ametsoc.org/view/journals/bams/96/2/bams-d-13-00167.1.xml>
 427 (Publisher: American Meteorological Society Section: Bulletin of the American
 428 Meteorological Society) doi: 10.1175/BAMS-D-13-00167.1
- 430 Shindell, D. T. (2014, April). Inhomogeneous forcing and transient climate
 431 sensitivity. *Nature Climate Change*, 4(4), 274–277. Retrieved 2021-
 432 09-10, from <http://www.nature.com/articles/nclimate2136> doi:
 433 10.1038/nclimate2136
- 434 Smith, C. J., Kramer, R. J., Myhre, G., Alterskjær, K., Collins, W., Sima, A.,
 435 ... Forster, P. M. (2020, January). *Effective radiative forcing and ad-*
 436 *justments in CMIP6 models* (preprint). Radiation/Atmospheric Mod-
 437 ellng/Troposphere/Physics (physical properties and processes). Retrieved
 438 2020-02-05, from <https://www.atmos-chem-phys-discuss.net/acp-2019-1212/> doi: 10.5194/acp-2019-1212
- 440 Sobel, A. H. (2002). The ENSO Signal in Tropical Tropospheric Temperature.
 441 *JOURNAL OF CLIMATE*, 15, 5.
- 442 Wood, R., & Bretherton, C. S. (2006, December). On the Relationship be-
 443 tween Stratiform Low Cloud Cover and Lower-Tropospheric Stability.
 444 *Journal of Climate*, 19(24), 6425–6432. Retrieved 2019-09-16, from
 445 <https://journals.ametsoc.org/doi/full/10.1175/JCLI3988.1> doi:
 446 10.1175/JCLI3988.1
- 447 Zelinka, M. D., Myers, T. A., McCoy, D. T., Po-Chedley, S., Caldwell,
 448 P. M., Ceppi, P., ... Taylor, K. E. (2020). Causes of Higher Cli-
 449 mate Sensitivity in CMIP6 Models. *Geophysical Research Letters*,
 450 47(1), e2019GL085782. Retrieved 2020-05-12, from <https://agupubs.onlinelibrary.wiley.com/doi/abs/10.1029/2019GL085782> (.eprint:
 451 <https://agupubs.onlinelibrary.wiley.com/doi/pdf/10.1029/2019GL085782>) doi:
 452 10.1029/2019GL085782
- 454 Zhou, C., Zelinka, M. D., & Klein, S. A. (2016, December). Impact of decadal cloud
 455 variations on the Earth's energy budget. *Nature Geoscience*, 9(12), 871–874.
 456 Retrieved 2021-10-12, from <http://www.nature.com/articles/ngeo2828>
 457 doi: 10.1038/ngeo2828
- 458 Zhou, C., Zelinka, M. D., & Klein, S. A. (2017). Analyzing the dependence of
 459 global cloud feedback on the spatial pattern of sea surface temperature change

460 with a Green's function approach. *Journal of Advances in Modeling Earth*
461 *Systems*, 9(5), 2174–2189. Retrieved 2021-06-17, from <https://agupubs.onlinelibrary.wiley.com/doi/abs/10.1002/2017MS001096> (.eprint:
462 <https://agupubs.onlinelibrary.wiley.com/doi/pdf/10.1002/2017MS001096>) doi:
463 10.1002/2017MS001096
464

Figure 1.

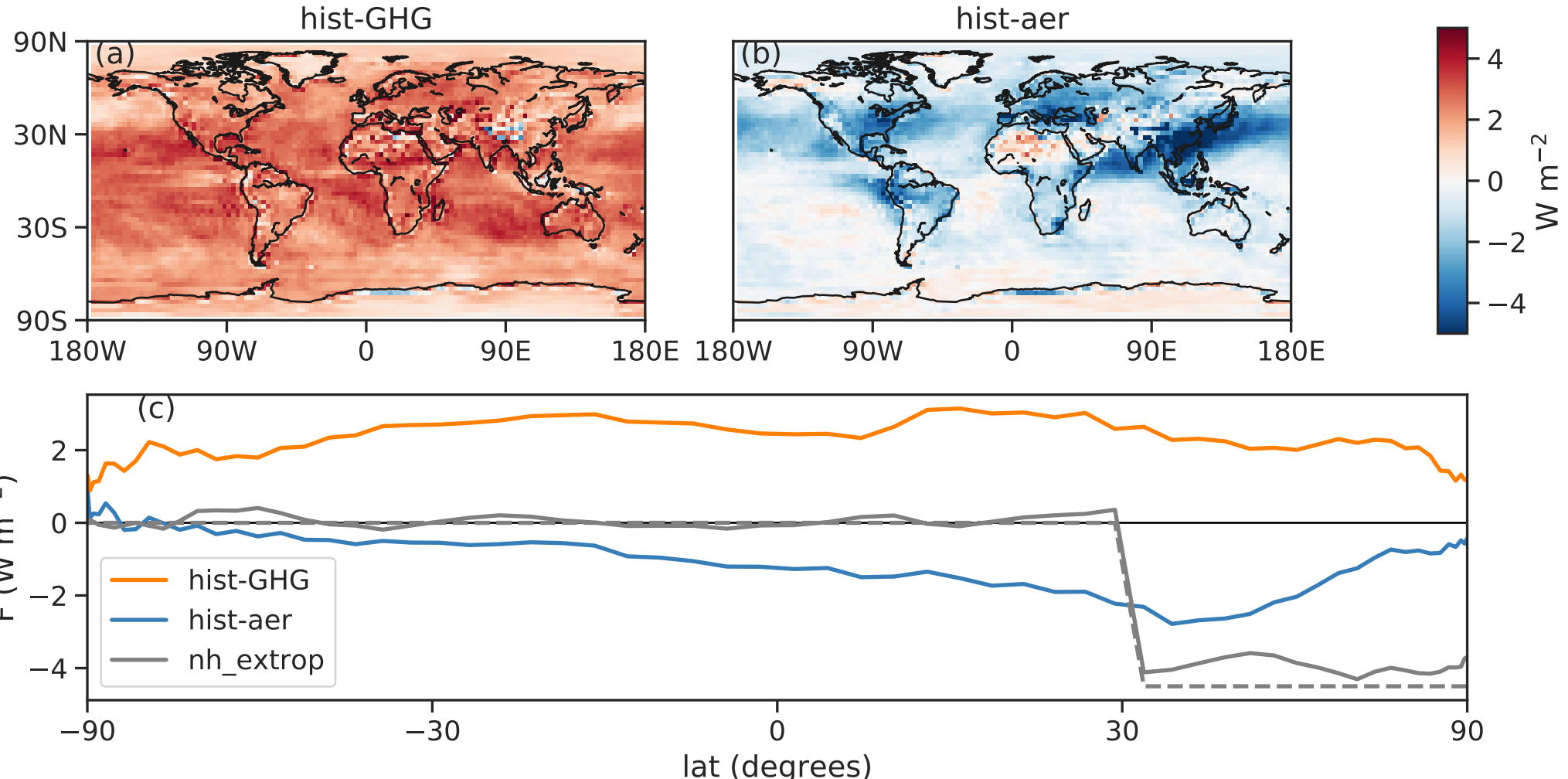
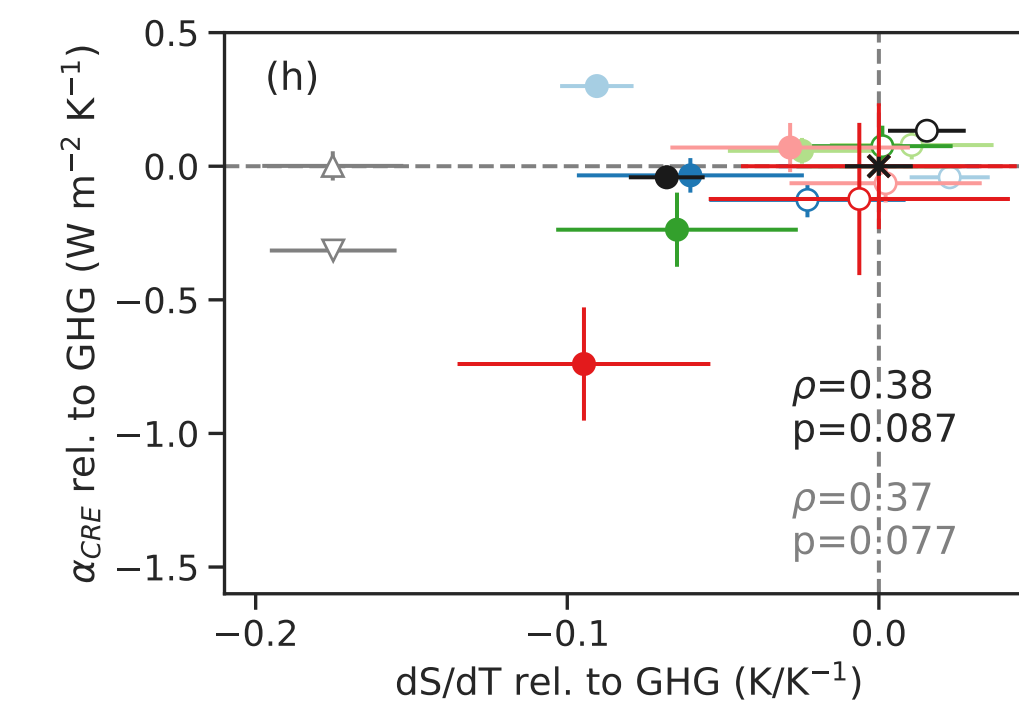
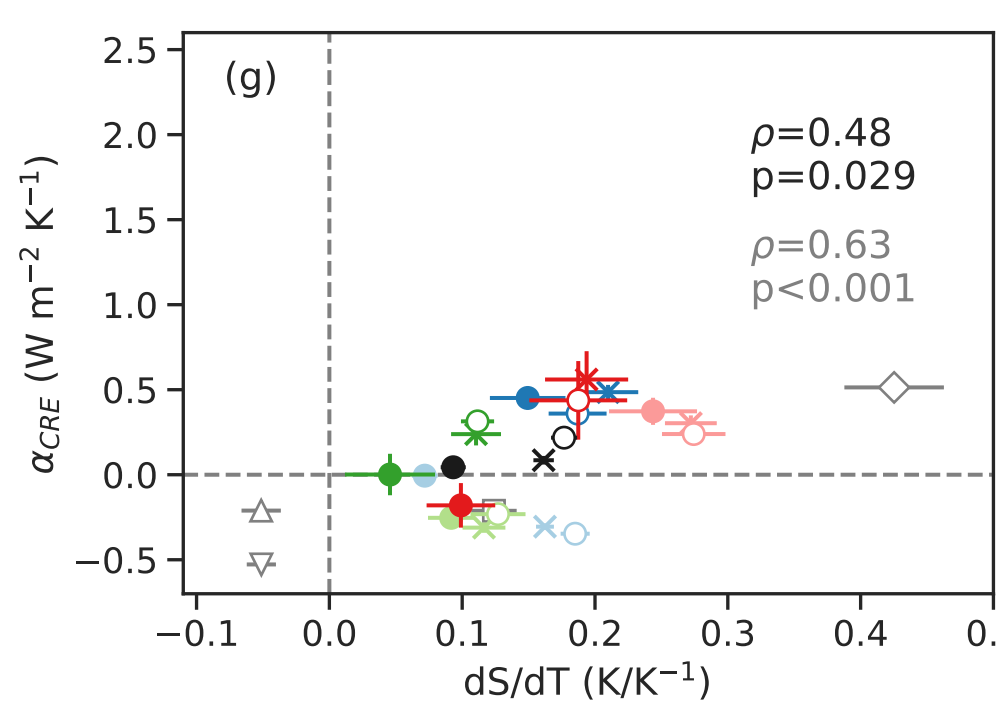
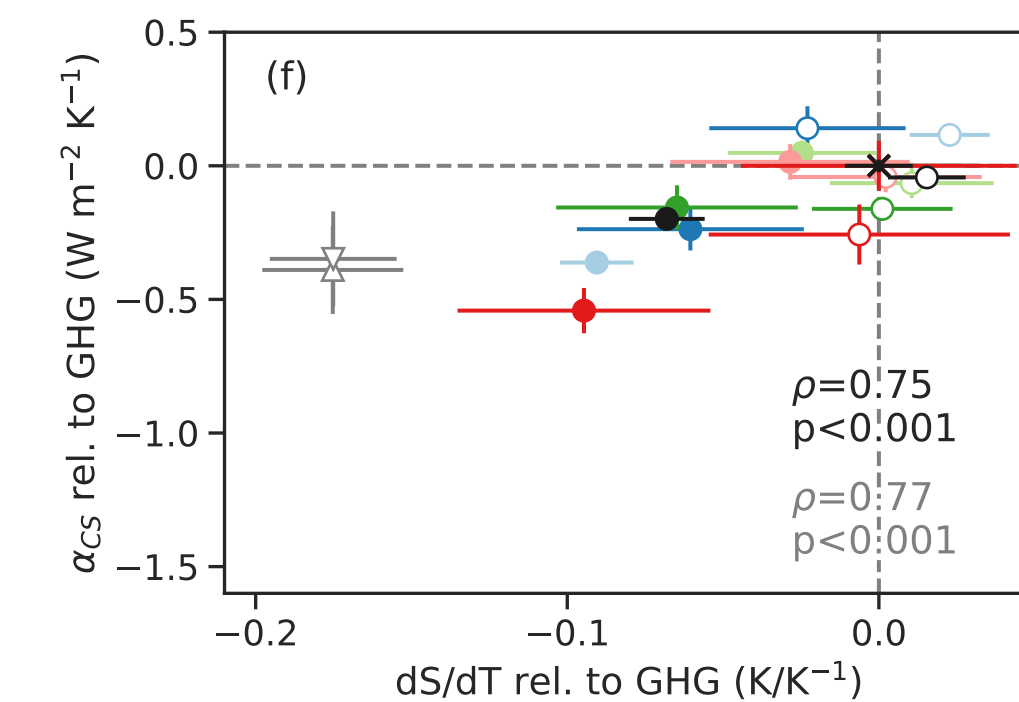
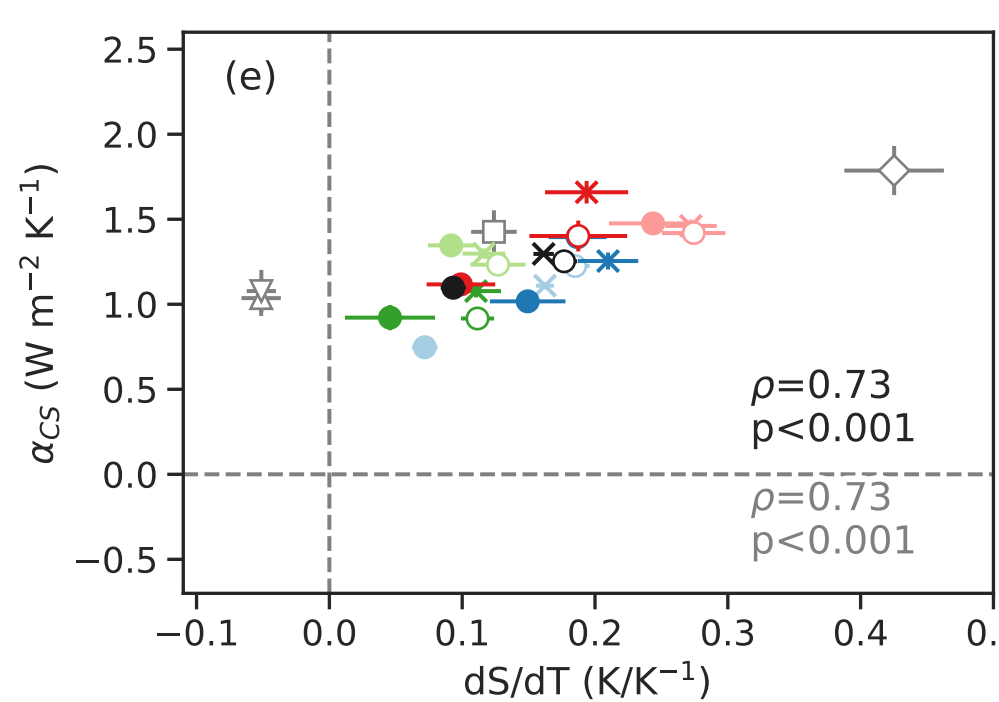
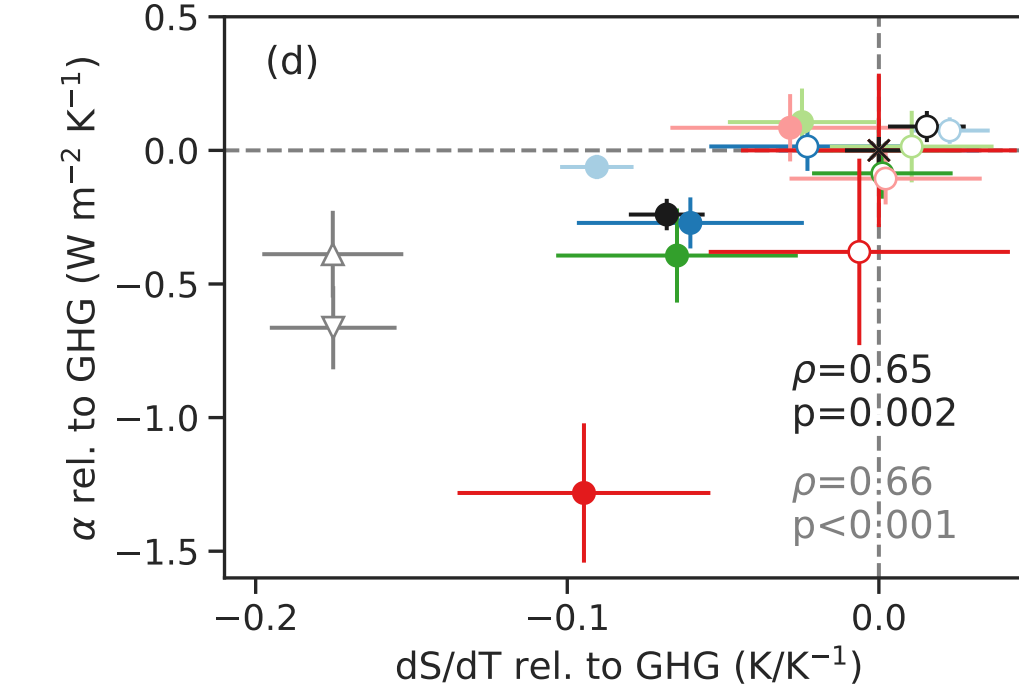
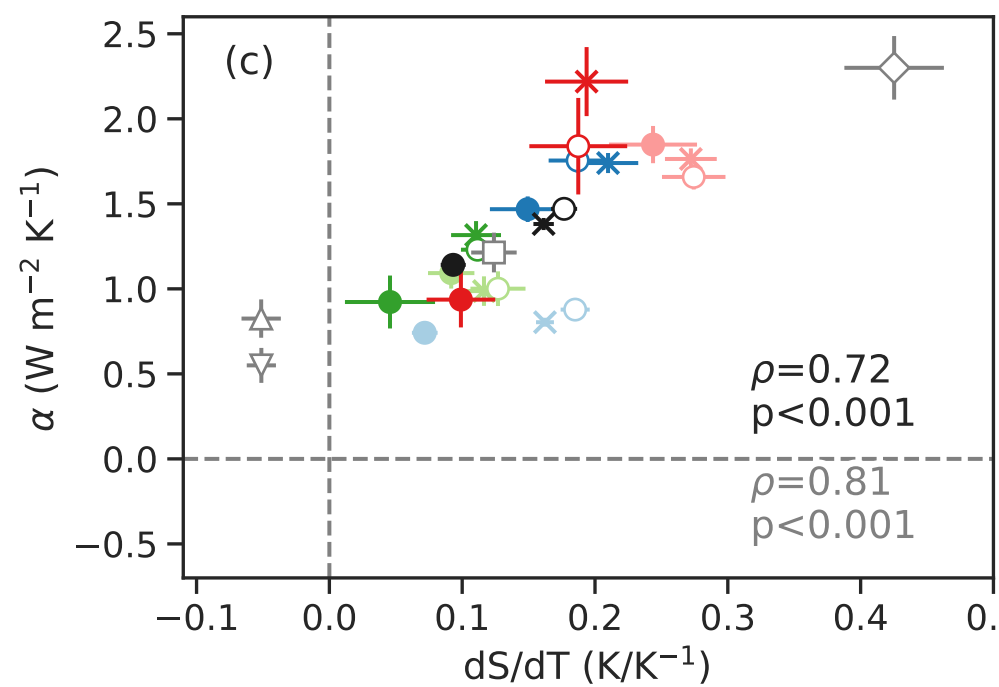
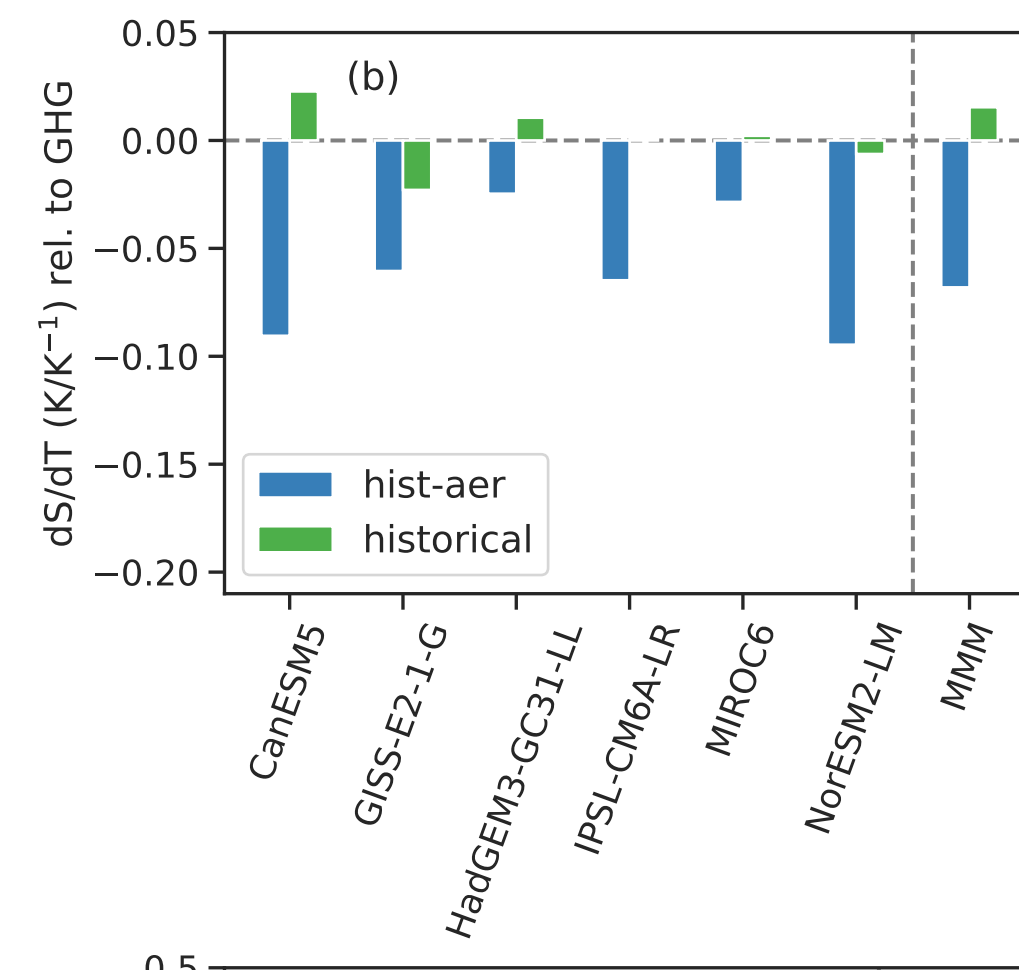
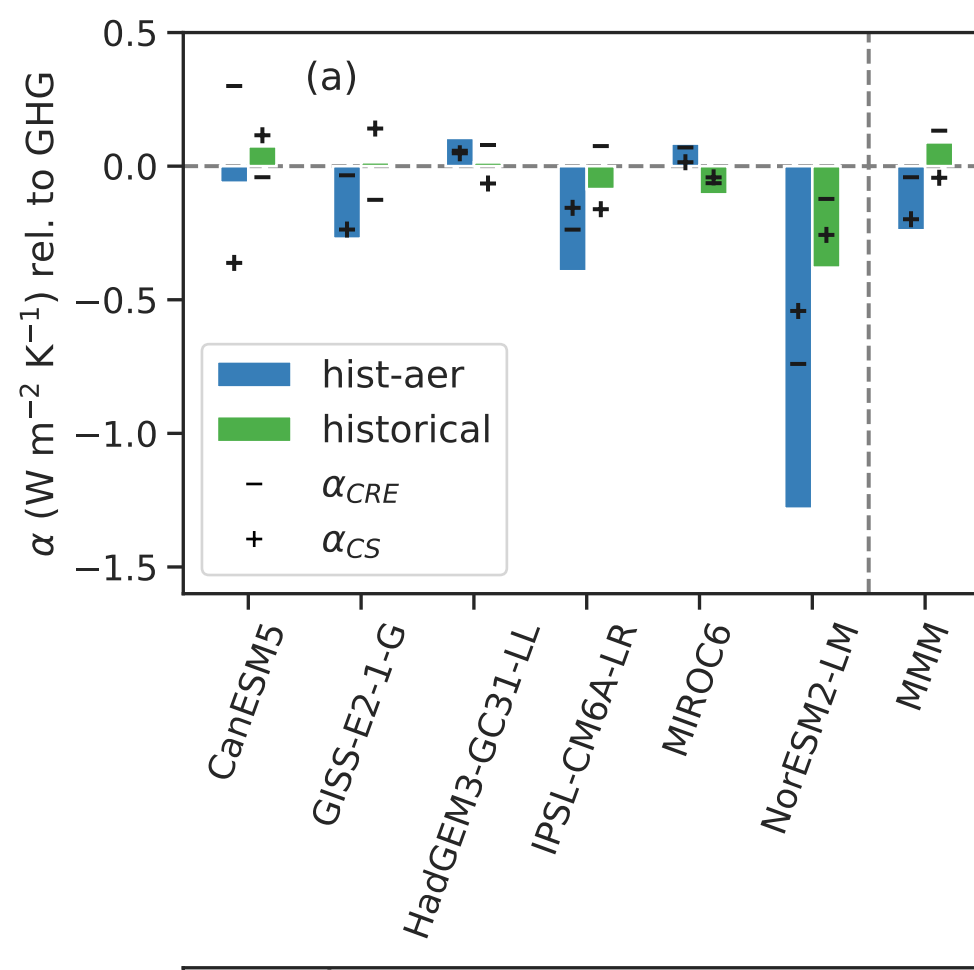


Figure 2.



key for panels (c-h)

CanESM5	GISS-E2-1-G	HadGEM3-GC31-LL	IPSL-CM6A-LR	MIROC6	NorESM2-LM	MMM
hist-aer	hist-GHG	historical	extrop_nh	extrop_sh	2xco2	tropical

Figure 3.

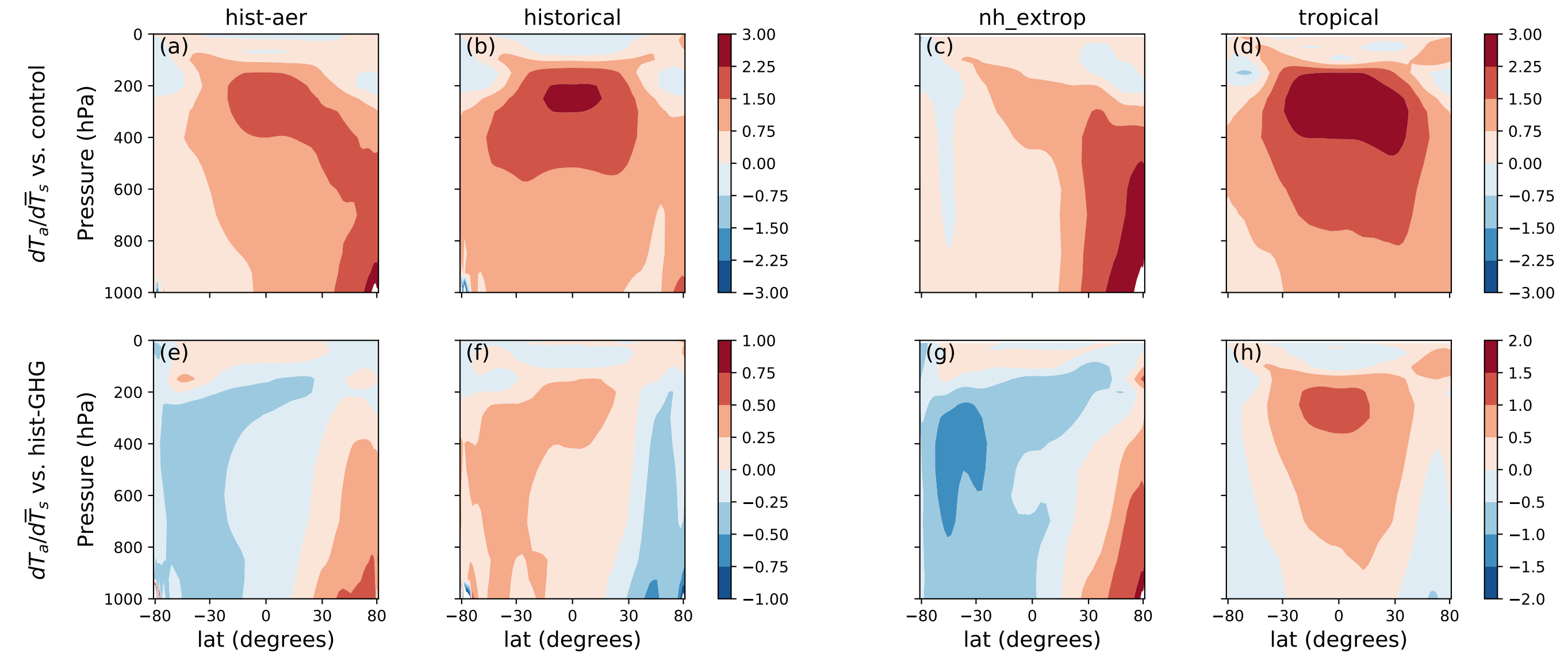


Figure 4.

